energy&fuels

pubs.acs.org/EF Article

Molecular Modeling and Adsorption Characterization of Micro-Mesoporous Kerogen Nanostructures

Shivam Parashar, Peter I. Ravikovitch, and Alexander V. Neimark*

Cite This: https://doi.org/10.1021/acs.energyfuels.2c02876 Read Online

ACCESS | Metrics & More | Article Recommendations | Supporting Information

ABSTRACT: The aim of this work is to enhance the understanding of the pore structure and adsorption properties of kerogens as applied to organic-rich shales and mudstone rocks. Conventional methods of adsorption characterization from low-temperature N_2 isotherms rely on the use of the so-called standard isotherms on nonporous substrates (typically silica or amorphous carbons), which may not be accurate for the surfaces of kerogens. In this work, we present a new methodology for pore size characterization of kerogens that relies on a realistic molecular model of kerogen surfaces. Taking advantage of recent advances in modeling the molecular structure of kerogens, we create atomistic three-dimensional (3D) models of amorphous bulk kerogens, rough kerogen surfaces, and mesopores imbedded in the amorphous kerogen matrix. Using grand canonical Monte Carlo (GCMC) simulations, we calculate the reference N_2 adsorption isotherms in the micropores of the bulk kerogen matrix, on the kerogen surface, as well as in a series of mesopores confined by rough kerogen walls. Next, we parameterized the quenched solid density functional theory (QSDFT) to reproduce the kerogen surface heterogeneity and GCMC-simulated N_2 adsorption isotherms. Furthermore, we approximated the isotherm on the reference kerogen surface by a macroscopic disjoining pressure isotherm, which allows us to use the Derjaguin−Broekhoff−de Boer (DBdB) model to predict adsorption and capillary condensation in meso/macropores. The reference GCMC, QSDFT, and DBdB isotherms are combined into the kernel for calculating the micropore volume, meso- and macropore surfaces, and mesopore size distribution from the experimental adsorption isotherms. The proposed methodology is demonstrated on a typical example of a kerogen II-A sample with a wide mesopore size distribution. The methodology can be extended to other kerogen structures of different maturities to provide a comprehensive characterization of organic porosity in kerogen fractions.

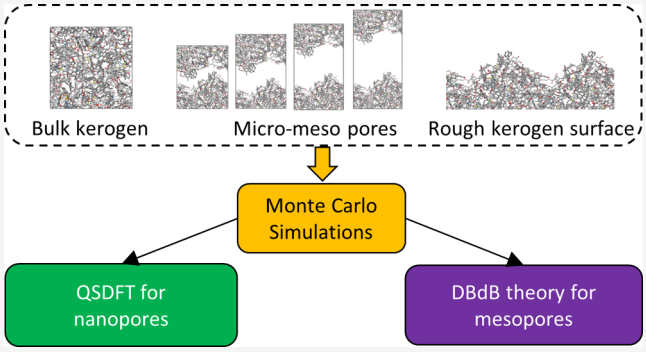

■ INTRODUCTION

The long-term growth of natural gas production in the United States comes from shale gas and associated gas from tight oil plays. The latter contributes a major part of the total natural gas production. Organic shales are simultaneously the source and reservoir rock for these unconventional resources. Shales are fine-grained low-permeability sedimentary rocks consisting of inorganic and organic fractions. Detailed characterization of the pore structure of shales is challenging due to heterogeneity and a wide pore size distribution spanning from μm down to nm size range.[1,2] Kerogen, by definition, is an insoluble fraction of organic matter in shales. It is a carbonaceous amorphous matter with the chemical composition (H/C and O/C ratios), density, and mechanical properties that depend strongly on the level of maturity.

A reliable pore structure characterization of kerogen is critical for understanding and predicting the hydrocarbon capacity, connectivity, and transport properties of shale reservoirs. The presence of organic porosity in kerogen has been well documented in the literature using, for instance, various microscopy techniques; however, quantification remains challenging due to the limited resolution. For the gas shales, helium-ion microscopy and small-angle neutron scattering identified the presence of "foamy porosity" and small bubble-like pores down to nm size, which are largely outside of the range of conventional scanning electron microscopy or mercury intrusion techniques (see, e.g., King et al.[2]).

An adsorption method is the most practical method for evaluating porosity, surface area, and pore size distribution from the experimental adsorption isotherms of nitrogen, argon, or carbon dioxide used as molecular probes. However, calculations of structural parameters require specific models of the pore structure and the adsorption process. While the conventional methods of pore structure analysis, such as

Received: August 28, 2022
Revised: October 4, 2022

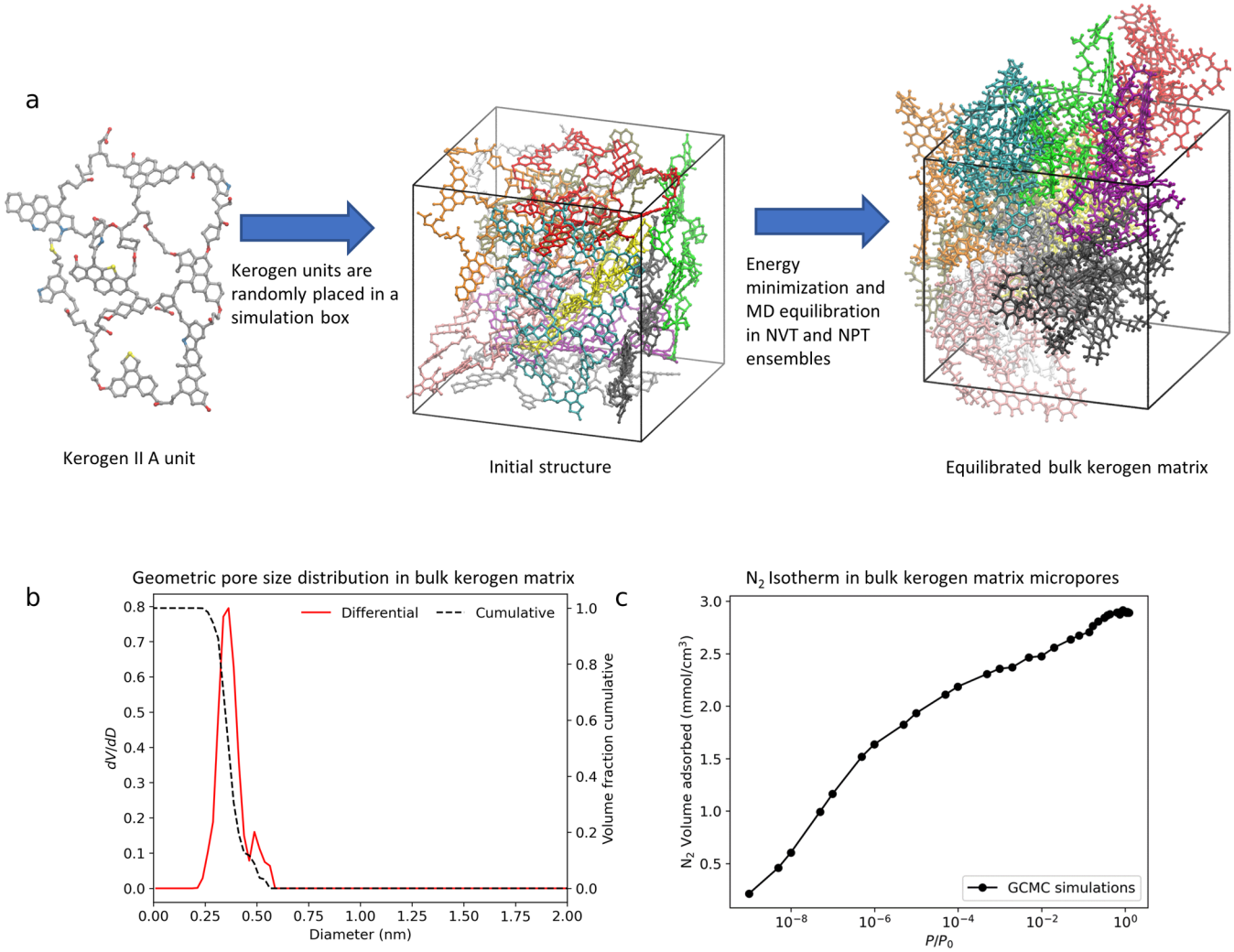

Figure 1. Construction of the molecular model of bulk kerogen and MC simulation of the bulk reference isotherm. (a) Creating the bulk kerogen matrix structure starting from 11 kerogen II-A units[10,21] (b) Differential (red) and cumulative (black dashed line) geometric pore size distribution of the equilibrated bulk kerogen matrix. (c) Reference GCMC adsorption isotherms of N_2 on the equilibrated bulk kerogen matrix.

Brunauer–Emmett–Teller (BET), for calculating the specific surface area, and Barrett–Joyner–Halenda (BJH), and more recent molecular model-based density functional theory (DFT) methods have been used for characterization of shales,[3−7] it should be recognized that existing adsorption models have limitations. In particular, models for calculating pore size distributions rely on the use of the so-called standard isotherms on nonporous substrates, which are typically silica, graphitic, or amorphous carbon surfaces, which may not be (and likely are not) an accurate representation of the kerogen surfaces. This is especially true for the low-maturity and oil-window kerogens as the interactions with the fluid are weaker because of the lower density of carbon atoms. Owing to the low surface areas and porosity, an accurate representation of adsorption on the surface is required for adsorption characterization.

In this work, we hypothesize that the pore structure of kerogen can be represented as a network of mesopores distributed in the microporous kerogen matrix. We present a new methodology for pore size characterization of kerogens that relies on a realistic molecular model of kerogen surfaces. There are several approaches in the literature to develop molecular level models of the kerogen structure. In the simplest case, the kerogen structure was modeled as graphitic slit pores, which is strong simplification.[8] Eberle et al.[9] modeled increased CH_4 confinement in nm-sized "foamy porosity" of gas shales using a spherical pore model with amorphous carbon walls of density matching that of mature kerogen. Chemically detailed molecular models of kerogen units were developed by Ungerer and co-workers[10] by matching the elemental fraction and number of functional groups obtained from X-ray photoelectron spectroscopy (XPS) and NMR data.[11] Six models of main types of kerogen units (I-A, II-A, II-B, II-C, II-D, III-C) were created corresponding to different maturity and the place of origin. These models were validated by matching the thermodynamic properties (like heat capacity, and absolute entropy) of the experimental kerogen samples with the quantum chemistry calculation. Ungerer's model has become popular for simulating molecular structures of the kerogen microporous matrix with embedded mesopores and modeling adsorption of N_2, CH_4, and CO_2.[9−12] Bousige et al.[1] created a bulk kerogen matrix model by matching not only chemical composition but also the structure factor, vibrational/mechanical properties, and density of samples. The authors used the molecular dynamics–hybrid reverse Monte Carlo (MC) method to create four kerogen models with different

https://doi.org/10.1021/acs.energyfuels.2c02876
Energy Fuels XXXX, XXX, XXX−XXX

maturities. Their structure predicts that CO_2 derived pore size distributions, vibrational density of states, and stiffness compared to experiments. Using this model, hydrocarbon (from methane to dodecane) transport was studied.[13] Phan et al.[14] modeled the transport of CO_2−CH_4 and H_2S−CH_4 mixtures in kerogen representing the kerogen micropore fragment by packing benzene molecules in a gap between flat silica surfaces. More elaborated structural models are presented by Liu and Chapman,[15] who studied hydrocarbon dissolution in the kerogen matrix modeled as a packing of asphaltenes and adsorption in slit pores with rough pore walls to represent mesopores.

In this work, we suggest a new methodology for characterization of kerogen pore structures based on implementation of the 3D molecular models into the practical theoretical methods of pore size distribution calculations, such as Derjaguin−Broekhoff−de Boer (DBdB)[16,17] and quenched solid density functional theory (QSDFT) methods.[18,19] This implementation allows for pore size distribution calculations in the whole range of pore sizes from micropores (<2 nm) to mesopores (2−50 nm) to marcopores (>50 nm) that are present in hierarchical kerogens. Using Ungerer's model of Kerogen II-A,[10] we create molecular structures of kerogen pores and by grand canonical Monte Carlo (GCMC) simulations, the reference adsorption isotherms of N_2 in the bulk microporous kerogen matrix, on the kerogen surface, and in slit pores of different sizes between molecularly rough kerogen surfaces. These reference isotherms are used for (a) constructing a bespoke QSDFT model of the mesopore pore walls and (b) parameterizing the disjoining pressure isotherm of the adsorption film on the kerogen surface for the DBdB model. The parameterized QSDFT and DBdB models verified against GCMC simulations are further used for predicting adsorption−desorption hysteretic isotherms in slit-shaped and cylindrical kerogen mesopores in the wide range of pore sizes from 1 to 10 nm. An original computational scheme is designed for calculating the pore size distributions from experimental isotherms that considers the hierarchical nature of the kerogen pore structure. The proposed method is illustrated on the pore structure characterization of a sample of Kimmeridge kerogen.[20]

■ METHODOLOGY

Creating Bulk Kerogen Structure. To study the adsorption properties of kerogen at the molecular scale, we constructed a bulk structure using Ungerer's molecular models of kerogen units.[10,21] As a case-study example, we consider II-A kerogen, which is rich in hydrogen and low in carbon, and it is formed from mixed terrestrial and marine source materials.[20,22] Kerogen II-A unit (Figure 1a) contains 252 carbon atoms with molecular formula $C_{252}H_{294}O_{24}N_6S_3$. Around 40% of the carbon atoms are a part of an aromatic ring, and on average, 11.4 carbon atoms constitute one aromatic cluster.[10] The oxygen atoms are located in ether bridges, carbonyl, hydroxyl, and carboxylic groups, whereas the nitrogen atoms are present as thiophenic and pyridinic rings. Sulfur is present in aromatic rings as sulfides and thiols.

To generate the bulk kerogen matrix, we place 11 kerogen II-A units in a simulation box (Figure 1a) in a random orientation. Energy minimization of the structure is followed by molecular dynamics (MD) simulations in NVT and NPT ensembles at 900 K and subsequently reducing the temperature to 300 K (see Table S3 in the Supporting Information). MD simulations are performed using the general amber force field (GAFF)[23] in LAMMPS.[24] The atomic charges were calculated using the charge equilibration method[25] implemented in RASPA.[26] The final temperature and pressure (300 K and 20 MPa) are characteristic to shale reservoirs.[21] The density of the equilibrated kerogen matrix (1.05 g/cm^3) is close to the density of experimental samples of kerogen II A.[27] The size of the corresponding simulation box is 40.732 Å.

The kerogen matrix represents a structure with intrinsic microporosity. To characterize the porosity, surface area, and pore size distribution in the equilibrated kerogen matrix, we use the geometric method implemented in Poreblazer.[28] The geometric method is based on sampling the molecular structure with virtual spherical probe particles of different sizes and constructing the Connolly surface enveloping the pores larger that the diameter of the probe. As shown in Figure 1b, the bulk kerogen matrix contains molecular size interstitial micropores in the range of 0.25−0.6 nm. The micropore volume determined by a "helium" probe is 0.12 cm^3/g, and the pore surface area determined by a "nitrogen" probe is 17.04 m^2/g. These geometric parameters reflect the specifics of the bulk kerogen microporosity. However, they should be used with a caution for predicting adsorption on practical samples due to potential micropore blockage by remaining hydrocarbons and limited accessibility.

Grand Canonical Monte Carlo (GCMC). The equilibrated structure of kerogen matrix is used to calculate the adsorption isotherms of N_2 using the GCMC simulations. The simulations are performed using the open-source software package RASPA.[26] A minimum of 100000 Monte Carlo moves are attempted for equilibration and averages over at least 200,000 moves are performed for production. The probabilities for molecule translation, rotation, reinsertion, and swap moves are 0.2, 0.2, 0.2, and 0.4, respectively. All of the isotherms are simulated at the N_2 normal boiling temperatures of 77.4 K. N_2 is modeled as a rigid three-center molecule described by the TraPPE force field.[29] Interaction parameters of the adsorbate with the framework atoms are computed using Lorentz−Berthelot mixing rules.[31] The LJ potentials for adsorbate interactions are truncated at 17 Å for N_2. Framework charges are obtained using the charge equilibration method,[25] and long-range electrostatic contributions are accounted with the Ewald summation method. The force field parameters for C, H, N, O, and S atoms are taken from the Dreiding force field,[30] which are summarized in Table S1 in the Supporting Information.

■ RESULTS AND DISCUSSION

Reference GCMC Isotherms on Bulk Kerogen. We perform GCMC simulations on the kerogen matrix to generate N_2 adsorption isotherms at their normal boiling temperature of 77.4 K (Figure 1c). This isotherm, N_{bulk}^{ref}, expressed per unit of kerogen matrix volume in mmol/cm^3 or per unit mass of kerogen in mmol/g, serves as the reference adsorption isotherm in kerogen micropores.

Modeling Kerogen Surface and Simulation of Reference Surface Isotherm. It is assumed that mesopores are embedded into the kerogen matrix. To model the mesopore surface and simulate the reference isotherm associated with surface adsorption, we consider a 10 nm slit pore confined by kerogen surfaces as 10 nm width is enough to diminish the interactions from the opposite walls. To build the molecular structure of the pore wall, we split the equilibrated bulk kerogen structure

https://doi.org/10.1021/acs.energyfuels.2c02876
Energy Fuels XXXX, XXX, XXX−XXX

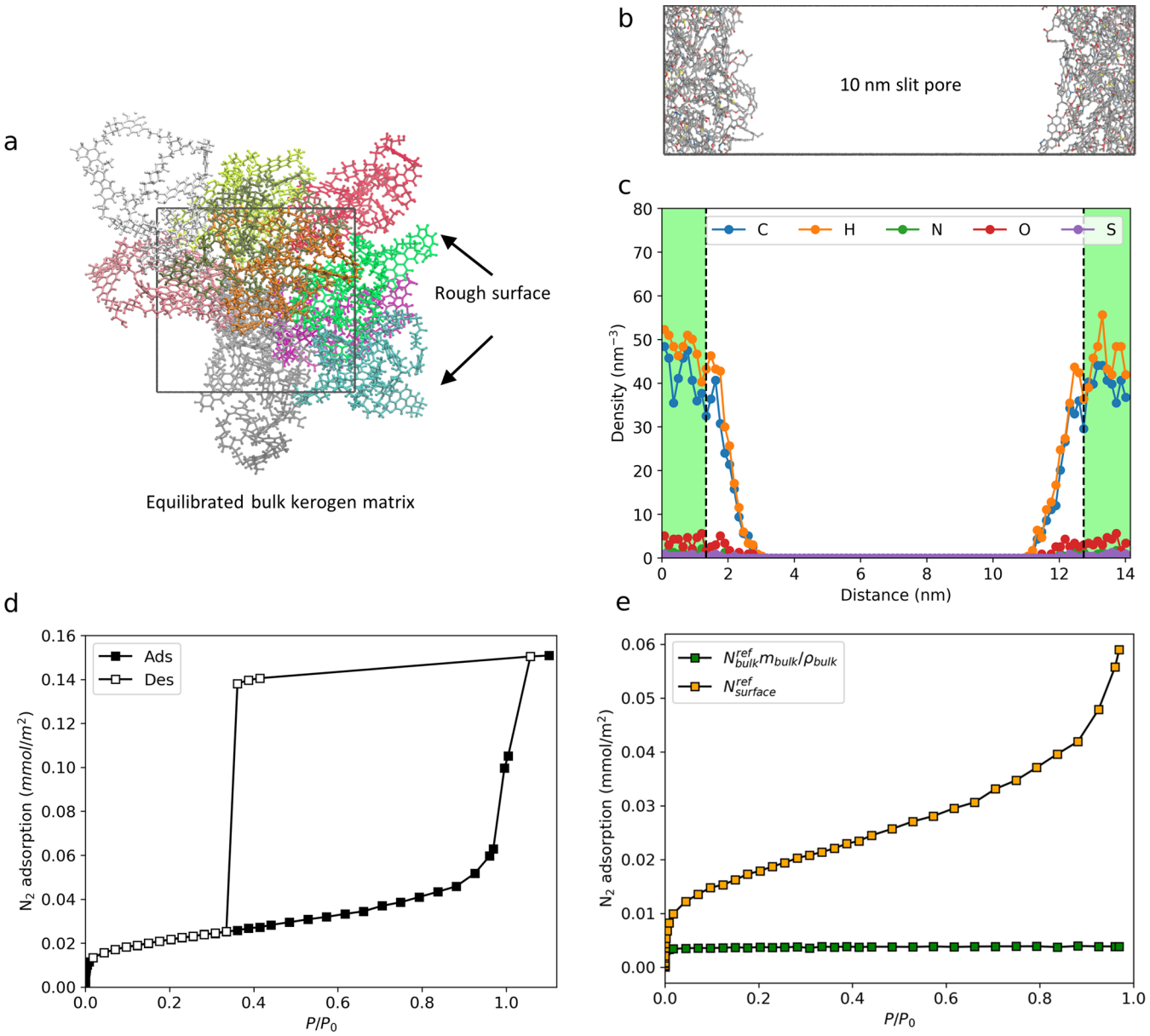

Figure 2. Construction of the molecular model of the kerogen surface and GCMC simulation of the surface reference isotherms. (a) Equilibrated kerogen matrix with a rough surface. (b) Snapshot of the molecular model of a 10 nm wide slit pore used for simulating the surface isotherm. (c) Density profiles of kerogen atoms along the slit pore. Broken lines separate the region of the bulk kerogen matrix of constant density (shaded in green) and the surface diffuse layer of varying density. (d) GCMC-simulated isotherm of N_2 in a 10 nm slit pore of kerogen. (e) Reference isotherm on the surface of kerogen $N^{ref}_{surface}$ and contribution of N_2 adsorption in the kerogen matrix $N^{ref}_{bulk} m_{bulk}/\rho_{bulk}$, which is proportional to the reference isotherm in bulk kerogen.

(Figure 2a) by introducing a space of 10 nm along the z direction without breaking any kerogen units. As shown in Figure 2b, the pore walls possess a rough surface due to different orientations of the kerogen units at the location of split. The density profiles of the kerogen atoms are shown in Figure 2c. The density of the kerogen wall at the surface gradually decreases from the density of bulk kerogen of ∼40 carbon atoms/nm^3 in the wall center to zero at the center of the pore. Extended equilibration of the pore wall molecular structure at 300 K provides slight fluctuations of density profiles along the simulation trajectory, which on average fit a linearly decaying ramp distribution. The pore wall can be divided into the central part of the bulk kerogen density and the diffused surface layer of decreasing density. The thickness of the bulk part is 1.3 nm, and the extension of the diffused surface layer is 1.4 nm. Using the terminology of QSDFT, the half-width of the diffused surface layer is called the roughness parameter, δ. The roughness parameter, δ = 0.7 nm, characterizes geometric inhomogeneity of the pore wall of the molecular level.

Figure 2d shows the N_2 adsorption isotherm at 77.4 K in a 10 nm slit pore calculated using GCMC simulations. The adsorption isotherm corresponds to the filling of the micropores in the kerogen wall at low pressure (P/P_0 < 0.01) and subsequent formation of the adsorption film on the pore surface that proceeds even beyond the saturation (P/P_0 > 1). Complete pore filling due to capillary condensation occurs above saturation due to an unsurpassable energy barrier in

https://doi.org/10.1021/acs.energyfuels.2c02876
Energy Fuels XXXX, XXX, XXX−XXX

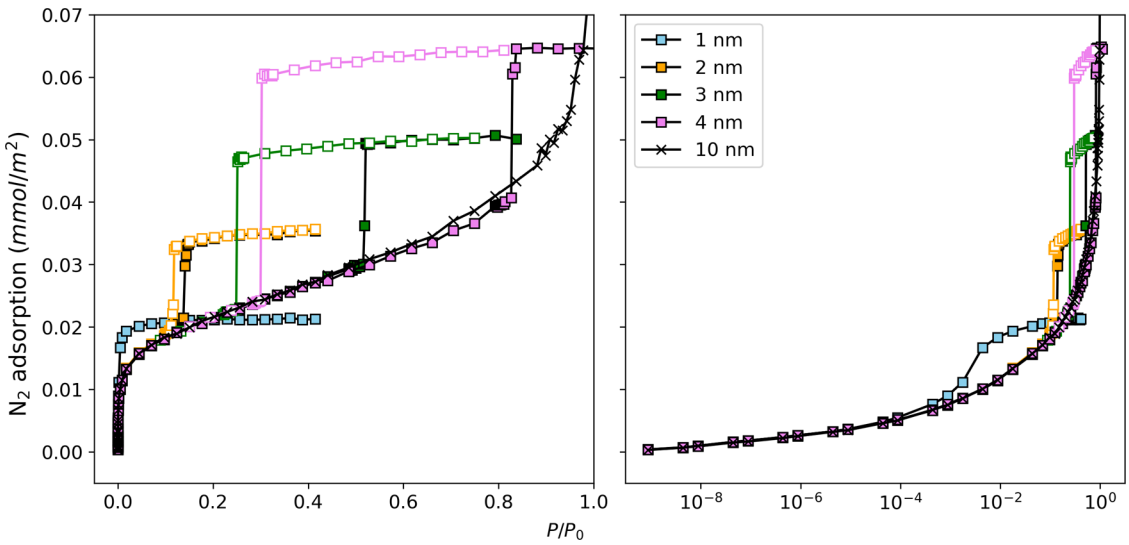

Figure 3. Comparison of the GCMC-simulated isotherms in slit pores of widths 1 (skyblue), 2 (orange), 3 (green), 4 (magenta), and 10 (black) nm. The 10 nm pore isotherm serves as the reference isotherm representing adsorption in the bulk kerogen matrix and on the surface of kerogen pores.

such wide pores. Note that this is characteristic to the experimental isotherms on kerogen, which commonly do not achieve a plateau at the saturation which indicates the existence of wide pores being unfilled.[20] The desorption isotherm exhibits a pronounced step that reflects evaporation of a condensed fluid via cavitation that is also characteristic of kerogen samples containing embedded mesopores.[20,32] The condensation and evaporation steps occur near $P/P_0 \sim 1$ and $P/P_0 \sim 0.35$, respectively, resulting in a wide hysteresis (Figure 2d).

The simulated adsorption isotherm in the 10 nm slit pore includes contributions from adsorption in the bulk region of the pore wall and on the rough surface. The former is proportional to the bulk reference isotherm and the latter to the surface reference isotherm. To extract the reference surface isotherm $N^{\mathrm{ref}}_{\mathrm{surface}}$ from the total GCMC isotherm N_{total} [mmol/m^2], we subtract the contribution from adsorption in matrix micropores shown by the shaded green region in Figure 2c,

$$N^{\mathrm{ref}}_{\mathrm{surface}} = N_{\mathrm{total}} - N^{\mathrm{ref}}_{\mathrm{bulk}} m_{\mathrm{bulk}}/\rho_{\mathrm{bulk}} \quad (1)$$

Here, $N^{\mathrm{ref}}_{\mathrm{bulk}}$ [mmol/cm^3] is the reference isotherm in the bulk kerogen shown in Figure 1c, m_{bulk} [g/m^2] is the mass of the kerogen wall per unit area, and ρ_{bulk} [g/cm^3] is the density of the bulk kerogen structure in Figure 1a. The surface adsorption isotherm $N^{\mathrm{ref}}_{\mathrm{surface}}$ [mmol/m^2] is presented in Figure 2e together with the respective isotherm in the pore wall micropores. The constructed isotherm, $N^{\mathrm{ref}}_{\mathrm{surface}}$, is further employed as a reference surface isotherm for modeling adsorption in mesopores.

In Figure 3, we present the GCMC N_2 adsorption−desorption isotherms in the slit pores of sizes 1, 2, 3, and 4 nm with the molecularly rough walls. These pores are constructed with the same kerogen pore walls as the 10 nm pore (Figure 2b). The adsorption isotherm in the 10 nm pore is shown for comparison. The isotherms presented on a per unit area basis in mmol/m^2 display several noteworthy features. First, all isotherms exhibit a sharp step and coincide with each other for relative pressures less than 10^{-3}. This region corresponds to adsorption in the micropores of kerogen pore walls, which are the same for all pores. Second, the deviations from the 10 nm pore isotherm, which represent the sum of the reference bulk and surface isotherms, occur at the onset of the filling of the gap between the pore walls that is clearly seen on the isotherm plots in the semi-logarithmic scale. This similarity confirms that adsorption on the kerogen surface occurs in a similar manner regardless of the pore size, and with minimal interactions of the adsorbate with the opposite pore wall. Third, all isotherms, except for the smallest 1 nm micropore, are irreversible and exhibit a hysteresis loop with distinct capillary condensation and desorption steps. The condensation and evaporation steps are delayed because of the formation of the metastable state and restricted fluctuations in the GCMC simulations that are insufficient to cross the energy barrier between vapor-like and liquid-like states.

The vapor−liquid equilibrium pressure of a fluid confined to nanopores is lower compared to the bulk fluid. The position of the capillary condensation−desorption equilibrium is located somewhere between the GCMC condensation and evaporation steps, and it cannot be determined using the GCMC simulations. Applications of more advanced MC simulation methods, like the gauge cell mesocanonical ensemble MC (MCEMC),[33−35] or the Widom insertion method, the canonical ensemble (NVT),[36] require expensive simulations and, in the case of kerogen, are impractical due to relatively wide mesopores. Calculations of the adsorption and equilibrium isotherms in the wide range kerogen mesopores can be done using quenched solid density functional theory (QSDFT)[37,18] and Derjaguin−Broekhoff−de Boer (DBdB) theory,[16,17,38] parameterized and verified against the GCMC simulations. The bulk and surface kerogen isotherms determined by simulating adsorption in the 10 nm wide pore serve as the reference isotherms for modeling adsorption in nanopores of any size and shape.

It is interesting to compare the GCMC-constructed reference surface isotherm, $N^{\mathrm{ref}}_{\mathrm{surface}}$, with the standard Harkins−Jura (HJ) isotherm, or the *t*-curve of de Boer, that is used in the classical Barret−Joyner−Halenda (BJH) method for calculating the pore size distributions from experimental adsorption isotherms.[39] In doing so, we should note that the HJ isotherm is normalized by the BET area, that is, the BET

https://doi.org/10.1021/acs.energyfuels.2c02876
Energy Fuels XXXX, XXX, XXX−XXX

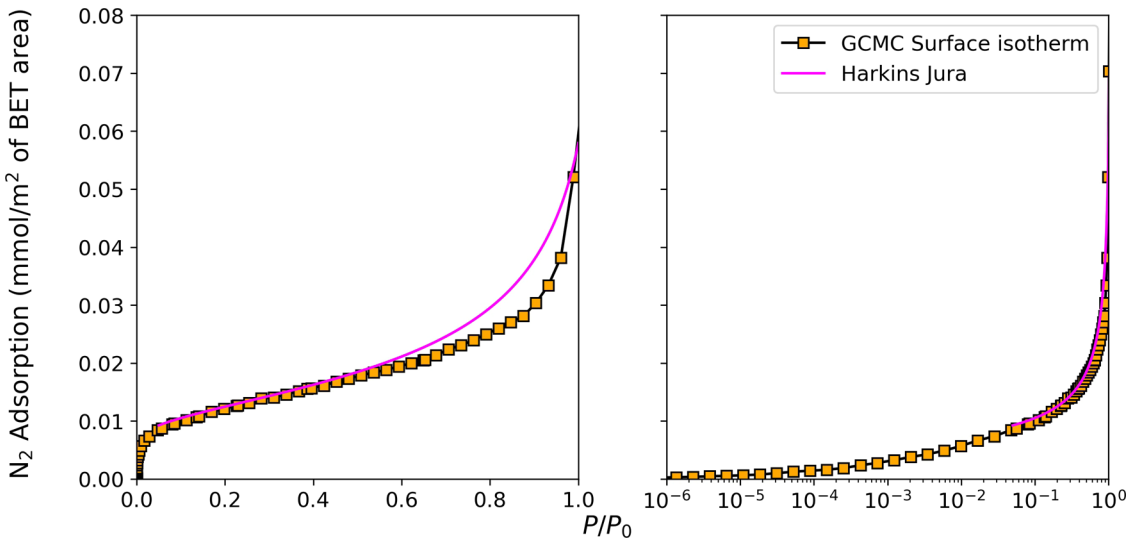

Figure 4. Comparison of the BET area-reduced GCMC kerogen surface isotherm and the standard Harkins–Jura isotherm.[39]

surface calculated from the HJ isotherm is 1 m^2. However, the HJ isotherm is considered as a reference isotherm of adsorption on a nonporous adsorbent, surfaces of which are not geometrically smooth. In contrast, the GCMC surface isotherm is normalized by the geometric area of the kerogen wall. Applying the BET method to the GCMC surface isotherm, one determines the ratio of the BET area of the kerogen wall to its geometric area S_{BET}/S_{geom} = 1.5. This factor effectively characterizes the surface roughness of kerogen, and compares to the inherent roughness of standard nonporous adsorbents used for verifying the HJ isotherm. In Figure 4, we compare the BET area-reduced GCMC surface isotherm, $N^{ref}_{surface}/(S_{BET}/S_{geom})$, and the HJ isotherm. After normalization, the isotherms practically coincide in the region $0.05 < P/P_0 < 0.5$. Deviations at higher pressures reflect the morphological and chemical specifics of the kerogen surface.

QSDFT Model of Kerogen Mesopores. Upon construction of the reference GCMC isotherms in the bulk kerogen and on the kerogen surface, our next step is to mimic these reference isotherms using the QSDFT model. QSDFT represents the adsorption system as a two-component mixture of solid and fluid (adsorbate) particles interacting via LJ potentials.[18,19,37] The solid matrix microporosity and pore wall surface roughness are accounted by the solid density distribution that is gradually reduced at the surface from the constant bulk solid density to zero. The near-surface layer of varying density is called the diffuse layer, and its extension is characterized by the roughness parameter, δ. The roughness parameter, δ, represents the half-width of the diffuse layer. A detailed description of the QSDFT model is given in section A of the Supporting Information.

QSDFT parameters are available for carbons and silica-based materials,[18,38] but they are unsuitable for kerogen because of its low density, which causes weaker interactions compared to activated carbons or graphite.[9] We use the atomistic structure and GCMC reference isotherm on bulk kerogen to parametrize the QSDFT model. The QSDFT parameters for modeling N_2 adsorption on kerogen are given in Table 1. A detailed description of how these parameters are calculated is discussed below using an example of a 3 nm slit pore.

In Figure 5a, we show the density profiles of kerogen components, C, H, N, O, and S, within a 3 nm wide slit pore

Table 1. QSDFT Parameters for a N_2 Kerogen System

parameters	value
roughness δ (nm)	0.7
fluid–fluid LJ parameters σ_{ff} (nm) and ϵ_{ff} (K)	0.3549 and 95.77
solid–fluid LJ parameters σ_{sf} (nm) and ϵ_{sf} (K)	0.269 and 150
hard sphere diameter of solid atoms d_{hs} (nm)	0.233
density of effective carbon atoms ρ_S^0 (nm^{-3})	66

and the atomistic structure of the kerogen pore walls in the background. The density profiles gradually reduce to zero within the diffuse layer near the surface. Since the QSDFT model operates with one type of solid particles, we introduce the density of the effective QSDFT solid particles by weighting the density profile of kerogen components by the ratio of the LJ energy parameters (Dreiding force field[30]) of the solid–fluid interaction, ϵ_{sf} to the respective LJ energy parameter for carbon, ϵ^C_{sf}, to obtain an equivalent density of effective solid particles, $\rho_S(z)$.

$$\rho_S(z) = \sum_i (\epsilon^i_{sf}/\epsilon^C_{sf})\rho_i(z) \tag{2}$$

Here, i is the kerogen components C, N, O, S, and H. We chose to represent the kerogen by effective carbon particles because it is the main constituent of kerogen and QSDFT interaction parameters of carbon with N_2 available in the literature.[18] The spatial variation of the solid density $\rho_S(z)$ is well approximated using the following linear ramp as shown in Figure 5b

$$\rho_S(z) = \begin{cases} \rho_S^0 & 0 \le z < w \\ \rho_S^0\left(\dfrac{z-w}{2\delta} - 1\right) & w \le z < w + 2\delta \\ 0 & w + 2\delta \le z < w + 2\delta + D/2 \end{cases} \tag{3}$$

Here, ρ_S^0 = 66 nm^{-3} is the density of bulk solid particles. Fitting the equivalent density of effective solid particles to the linear ramp in 3 allows us to define the QSDFT geometric parameters such as the pore diameter, D; surface roughness

https://doi.org/10.1021/acs.energyfuels.2c02876
Energy Fuels XXXX, XXX, XXX−XXX

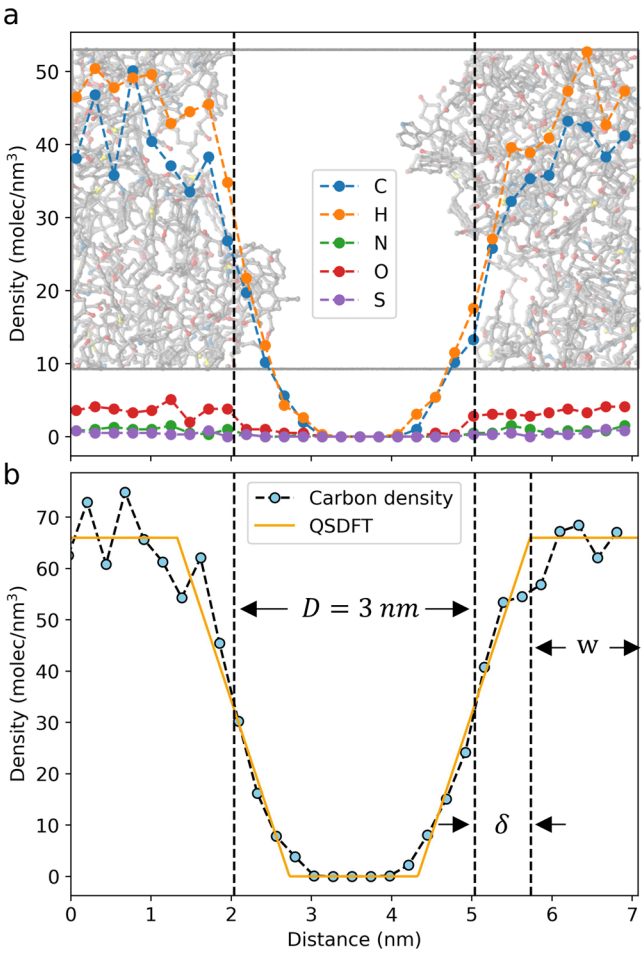

Figure 5. QSDFT model of a 3 nm kerogen slit pore. (a) Density profile of carbon, hydrogen, nitrogen, oxygen, and sulfur. Molecular structure of kerogen pore walls is shown in the background. (b) Density profile of carbon that mimics the solid−fluid interactions with five elements approximated by a linear density profile used in the QSDFT model.

parameter, δ; and bulk wall thickness, w. The pore diameter in QSDFT is defined according to the Gibbs rule of zero excess of solid particles that, in the slit geometry, equals to the distance between the points of half the maximum density. The roughness parameter, δ, is defined as the half-width of the linear ramp of the solid density profile. For the pore of diameter D = 3 nm, the roughness parameter, δ = 0.7 nm and the wall thickness, w = 1.3 nm (Figure 5b). The LJ potentials of fluid−fluid and solid−fluid are approximated according to the Weeks−Chandler−Andersen (WCA) scheme,[40] which, in addition, contains the LJ diameter, σ, accounting for particle attraction and the hard-core diameter, d, accounting for repulsion. While the fluid−fluid interaction parameters are taken from the literature,[18] the fluid−solid hard-core diameter, d_{hs} = 0.233 nm, was chosen to ensure that the adsorption capacity at P/P_0 = 1 within the bulk kerogen matrix is the same as calculated using the GCMC simulations.

In Figure 6, the QSDFT isotherms in the slit pores of sizes 1, 2, 3, 4, and 10 nm calculated with the parameters listed in Table 1 are compared with the GCMC isotherms. For all pores, the QSDFT and GCMC isotherms are well correlated in terms of the adsorption capacity and the positions of the pore fillings. These isotherms consistently show the transition from reversible to hysteretic isotherms as the pore size increases. In the smallest 1 nm micropore, the isotherm is reversible. The 2 mm pore is a borderline: the QSDFT isotherm exhibits a narrow hysteresis, while the GCMC isotherm is still reversible. In wider mesopores (>3 nm), the QSDFT and GCMC hysteresis loops practically coincide except for the positions of capillary condensation and desorption. Most importantly, QSDFT predicts the GCMC isotherms nicely during the adsorption film formation in mesopores from $P/P_0 \sim 10^{-2}$ up to the capillary condensation.

At low pressures, $P/P_0 < 10^{-3}$, QSDFT underpredicts the adsorption compared to GCMC, which can be seen in the semi-log plot for the 1 nm slit pore. The reason of this mismatch at low pressures is that the QSDFT model was parametrized with an objective to predict the adsorption on the surface and in slit pores with comparable accuracy to GCMC. Modeling the microporosity within the kerogen matrix using QSDFT is beyond the scope of this work and is not required for further analysis. The GCMC reference isotherm in the bulk kerogen matrix is sufficient to account for the adsorption in micropores.

As expected, the QSDFT adsorption−desorption isotherms in mesopores exhibit a wider hysteresis loop and predicts higher condensation pressure and lower desorption pressure compared to GCMC. This is explained by the fact that the DFT approach neglects the effects of density fluctuations, and the phase transition occurs at the spinodals. The positions of GCMC phase transitions are determined by the probabilities of nucleation and crossing the energy barriers; the wider the pore, the closer the spinodal transition occurs. This is clearly seen for a 10 nm pore with practically overlapping QSDFT and GCMC hysteresis loops. The advantage of the QSDFT is the ability to predict the equilibrium transition that is located between the condensation and desorption transitions. This allows us to construct the equilibrium adsorption isotherms that are used for calculating the pore size distributions from experimental adsorption isotherms.

Adopting the DBdB Method for Modeling Capillary Condensation and Desorption in Kerogen Mesopores. The DBdB theory presents surface adsorption as a layer of bulk fluid density, thickness t of which at given adsorbate pressure corresponds to the surface adsorption isotherm.

$$t(P/P_0) = V_L N^{ref}_{surface}(P/P_0) \quad (4)$$

Here, V_L is the bulk liquid molar volume. This representation in 4 is similar to the common definition of the adsorbed film thickness used in the t-curve of the de Bour method.[16] Thermodynamics of the adsorbed liquid film of thickness t is characterized by the disjoining pressure, $\Pi(t)$, which is determined from the condition of equality of chemical potentials in the adsorbed film and in the gas phase at given P.

$$\Pi(t) = -RT/V_L \ln(P/P_0) \quad (5)$$

5 implies that the adsorbed film is considered as a layer of homogeneous incompressible liquid in equilibrium with an ideal gas. In Figure 7, the GCMC reference isotherm is plotted in terms of disjoining pressure dependence on the effective film thickness, $\Pi(t)$ using 5. The GCMC disjoining pressure isotherm is approximated by an exponential function, $\Pi(t) = Ae^{-t/b}$, where $A = 2.2 \times 10^8$ Pa and b = 0.31 nm. A represents the strength of the solid−fluid interactions and b represents the

https://doi.org/10.1021/acs.energyfuels.2c02876
Energy Fuels XXXX, XXX, XXX−XXX

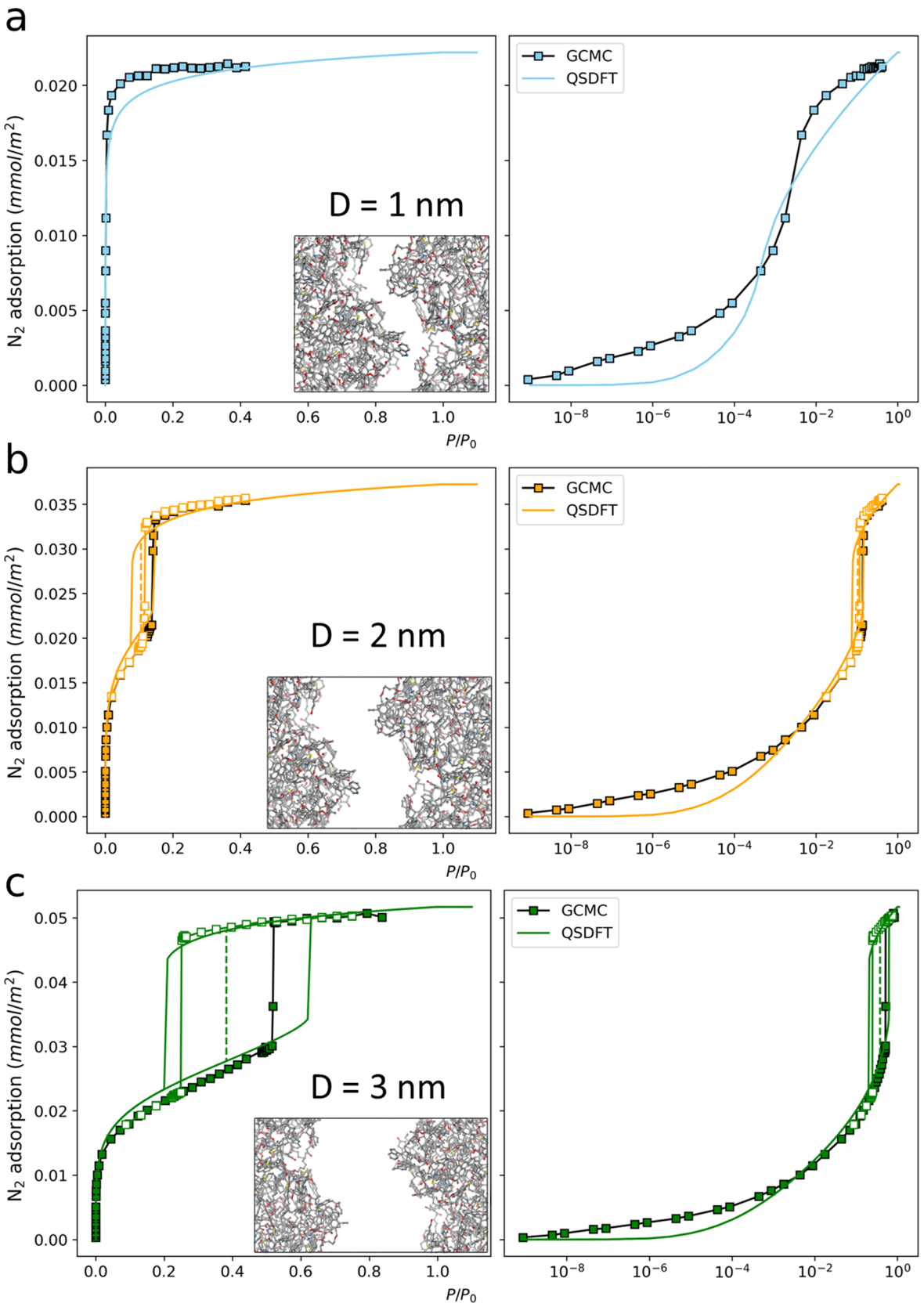

Figure 6. continued

https://doi.org/10.1021/acs.energyfuels.2c02876
Energy Fuels XXXX, XXX, XXX−XXX

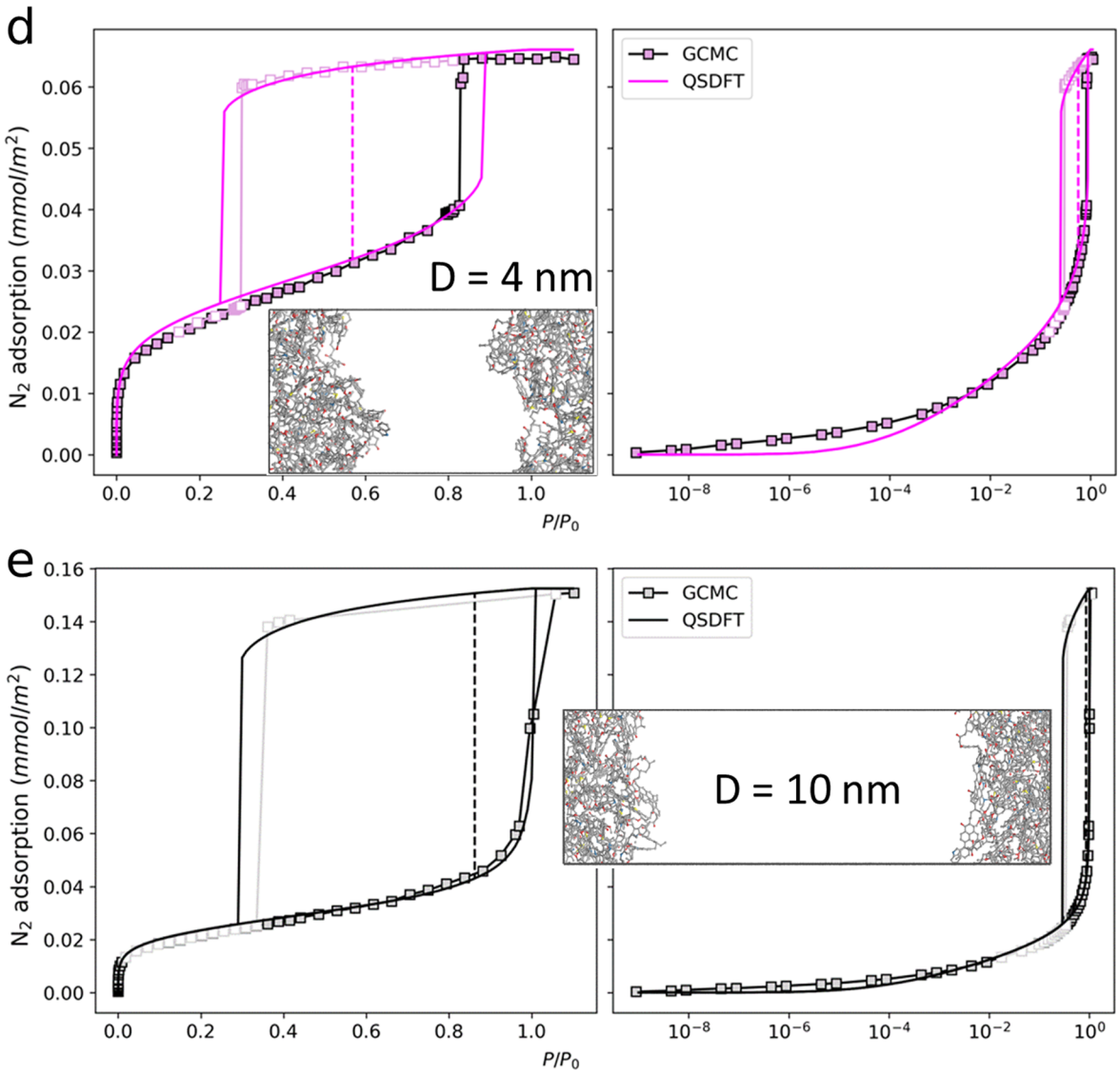

Figure 6. Comparison of N_2 isotherm computed using GCMC and QSDFT in slit pores of sizes (a) 1 nm (b) 2 nm (c) 3 nm (d) 4 nm, and (e) 10 nm. The vertical dashed lines are the equilibrium vapor−liquid transition pressures predicted by QSDFT.

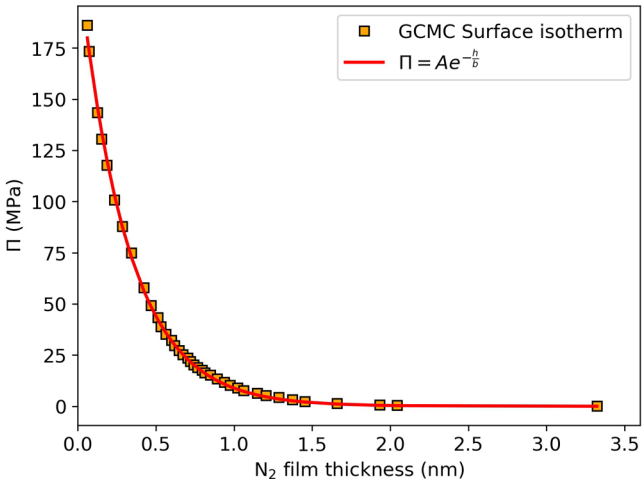

Figure 7. Disjoining pressure isotherm, $\Pi(t)$, for the kerogen surface constructed from the GCMC reference surface isotherm. Approximation by the exponentially decaying function, $\Pi(t) = Ae^{-t/b}$ (red).

decay length. This functional form of disjoining pressure is frequently used in the literature for different systems.[41−43]

The DBdB theory allows us to estimate the position of equilibrium capillary condensation and desorption in mesopores depending on the disjoining pressure isotherm, $\Pi(t)$, and the surface tension of liquid adsorbate, γ.[16,17] The DBdB condition for vapor−liquid equilibrium in a pore of given size, D, is given by the system of equations with respect to the equilibrium relative pressure, P/P_0, and respective adsorbed film thickness, t.

For slit pores,

$$\begin{cases} \Pi(t) = -(\mathrm{RT}/V_\mathrm{L})\ln(P/P_0) & (6) \\ \mathrm{RT}\ln(P/P_0) - \dfrac{V_\mathrm{L}}{D/2 - t}\displaystyle\int_t^{D/2}\Pi(t)\mathrm{d}t = -\dfrac{\gamma V_\mathrm{L}}{D/2 - t} & (7) \end{cases}$$

For cylindrical pores,

https://doi.org/10.1021/acs.energyfuels.2c02876
Energy Fuels XXXX, XXX, XXX−XXX

$$\begin{cases} \mathrm{RT}\ln(P/P_0) + \Pi(t)V_\mathrm{L} = -\dfrac{\gamma V_\mathrm{L}}{D/2 - t} & (8) \\ \mathrm{RT}\ln(P/P_0) - \dfrac{2V_\mathrm{L}}{(D/2 - t)^2}\displaystyle\int_t^{D/2}(r_\mathrm{p}-t)\Pi(t)\mathrm{d}t & (9) \\ \quad = -\dfrac{2\gamma V_\mathrm{L}}{D/2 - t} \end{cases}$$

Here, the pore size, D, represents the width of the slit pore and the diameter of the cylindrical pore, and the exponential function approximation of the disjoining pressure is used, $\Pi(t) = Ae^{-t/b}$. The DBdB approach neglects the dependence of the disjoining pressure on the pore wall curvature, and therefore, the disjoining pressure of the adsorbed film in the cylindrical pore does not depend on the pore size.

The DBdB theory represents an improvement over the Kelvin−Cohan (KC) equations, which constitute the basis of the conventional BJH method[44] for pore size distribution calculations. KC equations predict the equilibrium capillary condensation pressure from the condition of equilibrium meniscus without accounting for the solid−fluid interactions in the adsorbed film. The condition of equilibrium using KC equations represents Laplace−Kelvin equations for cylindrical and spherical menisci in slit and cylindrical pores, respectively.

$$\begin{cases} \mathrm{RT}\ln(P/P_0) = -\dfrac{\gamma V_\mathrm{L}}{D/2 - t} & (10) \\ \mathrm{RT}\ln(P/P_0) = -\dfrac{2\gamma V_\mathrm{L}}{D/2 - t} & (11) \end{cases}$$

The DBdB eqs 6 and 9, reduce to KC eqs 10 and 11 when the disjoining pressure, $\Pi(t)$, is neglected. Therefore, DBdB and KC equations asymptotically merge as the pore size increases. Note that KC eqs 10 and 11, require a certain reference adsorption isotherm expressed as the film thickness dependence on the relative pressure, $t(P/P_0)$. Commonly, the film thickness is calculated using the t-curve of the de Bour or Harkins−Jura (HJ) equation.[45] The latter is an universal isotherm that is applied for various solid surfaces disregarding of their chemistry and molecular structure.

The solution of the DBdB equations with the disjoining isotherm, $\Pi(t) = Ae^{-t/b}$, provides the sought pore size dependence of the equilibrium capillary condensation pressure in kerogen mesopores of slit and cylindrical shapes. The dependencies are given in Figure 8 in comparison with the respective QSDFT and KC dependencies. For both slit and cylindrical pores, QSDFT and DBdB agree perfectly even up to a small pore diameter of 2.5 nm. The KC equations with the standard HJ isotherm predict higher pore filling pressures compared to QSDFT and DBdB. Implementation of the GCMC reference isotherm on the kerogen surface in KC equations instead of the HJ isotherm provides a better prediction of pore filling pressures, still overestimates the equilibrium pressure.

The equilibrium DBdB isotherm in the pore of size D is calculated as following. In the region of the adsorbed film formation before the capillary condensation pressure, the isotherm is determined by the film thickness $t(P/P_0)$ defined from eq 6 for slit pores and from eq 8 for cylindrical pores. At the capillary condensation pressure, the isotherm exhibits a step and achieves a plateau corresponding to the complete pore filling with a liquid adsorbate of bulk density. The DBdB equilibrium isotherms for the pore sizes from 2 to 200 nm are further used a kernel for calculating the mesopore size distribution from experimental adsorption isotherms.

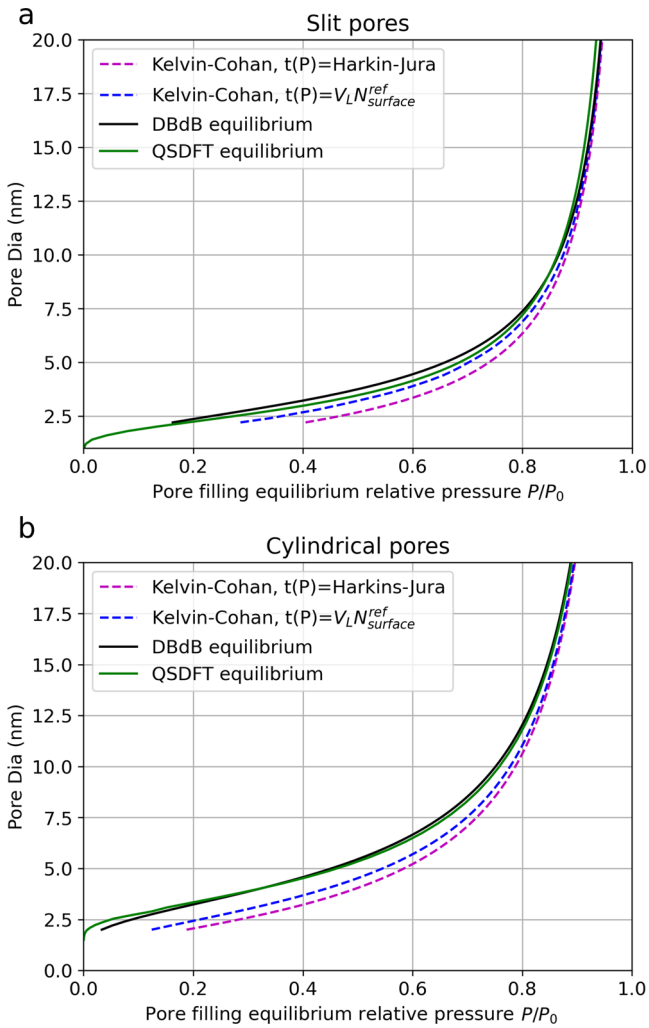

Figure 8. Comparison of the pore size dependencies of the equilibrium capillary condensation pressure predicted using QSDFT (green), DBdB (black), Kelvin−Cohan with Harkins−Jura film thickness isotherm (magenta), and with the GCMC reference surface isotherm (blue) for N_2 confined in (a) slit pores and (b) cylindrical pores.

Characterization of a Kimmeridge Kerogen Sample. The proposed methodology is illustrated on a typical example of the N_2 isotherm of a sample of Kimmeridge kerogen. Kimmeridge kerogen is extracted from the marine, clastic source rock consisting majorly type II kerogen with a pinch of type III and lies in the middle of the oil window.[22] The Kimmeridge isotherm (Figure 9a) is of type II by the IUPAC classification with a negligible hysteresis, insignificant uptake at low pressures that would be characteristic to filling of micropores. Note that the isotherm does not achieve a plateau that would correspond to the incomplete pore filling approaching the saturation. This behavior is typical for kerogen samples and suggests the existence for wide macropores (D > 50 nm) that are filled via a capillary condensation mechanism. The isotherm rise at $P/P_0 \rightarrow 1$ is due to continuing adsorption on the surfaces of unfilled pores. This factor is considered while calculating the pore size distributions.

https://doi.org/10.1021/acs.energyfuels.2c02876
Energy Fuels XXXX, XXX, XXX−XXX

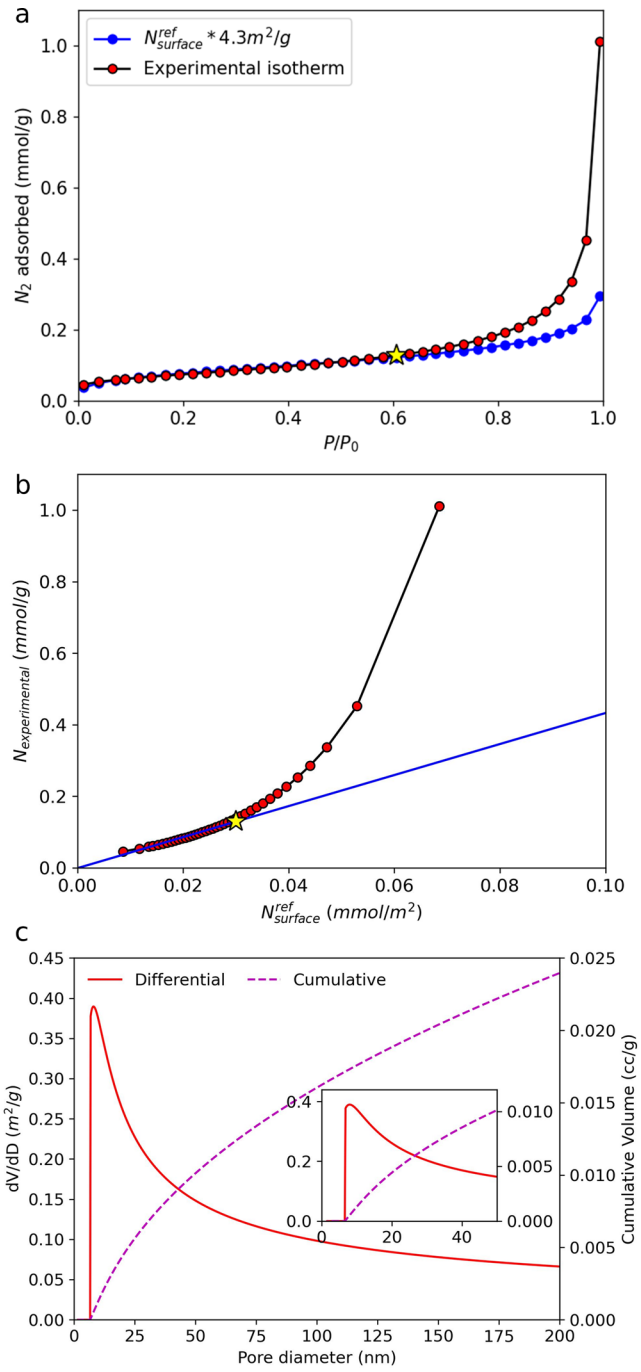

Figure 9. (a) Experimental isotherm of N_2 at 77 K on the Kimmeridge[20] kerogen sample (red squares) compared with the reference isotherm on the kerogen surface calculated using GCMC simulations. The yellow star shows the point after which the experimental isotherm deviates from the reference surface isotherm. (b) Calculation of the surface area and micropore volume of Kimmeridge kerogen[20] using a comparison plot method. The yellow star marks the point after which the experimental isotherm deviates from the reference surface isotherm. (c) Differential and cumulative pore size distributions of Kimmeridge kerogen calculated using the DBdB cylindrical pore kernel.

First, we determine the contributions from the micropore adsorption and adsorbed film formation in mesopores before the onset of capillary condensation. The comparison method allows us to calculate the micropore volume and mesopore surface area of the kerogen sample. In Figure 9b, we plot the experimental isotherm on Kimmeridge kerogen on y-axis against the reference surface isotherm, $N^{ref}_{surface}$, on the x-axis. The resulting comparison plot shows the correlation of the experimental isotherm with the reference surface isotherm. The linear part of the plot shows that the experimental isotherm is proportional to the reference surface isotherm up to $P/P_0 \sim 0.6$ (shown by yellow star); it is fitted by the blue straight line in Figure 9b. Since the reference surface isotherm is given per unit surface area, the slope of the linear part of the comparative plot equals to the total mesopore surface area of the sample available to N_2 adsorption. The y-axis intercept of the linear approximation represents the micropore volume. For this sample, the micropore volume is negligible, suggesting that kerogen micropores are not accessible for N_2 adsorption. The slope corresponds to the mesopore surface area of 4.3 m^2/g. This value is lower compared to the BET area of 6.6 m^2/g determined from the experimental isotherm. The reason is that the kerogen reference surface isotherm is calculated per geometric area of the kerogen surface, which is molecularly rough, and the area of 4.3 m^2/g represents the geometric area of the kerogen surface. The BET area is higher as it represents the effective area of the plain surface that would have the same adsorption as on the molecularly rough surface. The ratio, 6.6/4.3 = 1.5, characterizes the inherent roughness of the kerogen surface.

Upon scaling the $N^{ref}_{surface}$ by the surface area of 4.3 m^2/g determined from the comparison plot, we get a nice agreement with the experimental isotherm up to $P/P_0 = 0.6$, which is shown by yellow star in Figure 9a. The deviation of the experimental isotherm from the surface isotherm is due to the mesopore pore filling, and the point of $P/P_0 = 0.6$ is considered as the onset of capillary condensation in smallest mesopores of the sample. Based on the DBdB approach, $P/P_0 = 0.6$ corresponds to the filling pressure of 6.5 nm pores. This means that the smallest pores within this sample are of diameter D_{min} = 6.5 nm. For calculating the pore size distribution, we generated the kernel of reference isotherms in kerogen cylindrical mesopores composed of the equilibrium DBdB isotherms in the pores of different diameters, D_i, starting from 6.5 to 200 nm.

A sharp uptake in the experimental isotherm near saturation indicates that not all pores are filled at the last point of the isotherm. We assume that adsorption in the unfilled pores proceeds according to the reference surface isotherm. This contribution is accounted for by adding the surface isotherm to the kernel and calculating the pore size distribution, $f(D)$, and the surface of unfilled macropores, S_{ma}, from the modified generalized adsorption equation.

$$N_{exp}(P/P_0) = V_{mi}N^{ref}_{mi}(P/P_0) + \int_{D_{min}}^{D_{max}} K(P/P_0, D)f(D)\mathrm{d}D + S_{ma}N^{ref}_{surface}(P/P_0) \quad (12)$$

Equation 12 represents the experimental isotherm as the sum of the adsorption isotherms in micropores, mesopores, and on the surface of unfilled macropores. Here, N_{exp} (P/P_0) [mol/g] is the experimental isotherm, V_{mi} is the micropore volume, N^{ref}_{mi} is the reference isotherm in micropores, $f(D)$ [m^2/g] is the pore size distribution function, $K(P/P_0, D)$[mol/m^3] is the kernel of the isotherms measured in moles of N_2 adsorption per unit volume of the cylindrical pores, $N^{ref}_{surface}$ [mol/m^2] is the reference surface isotherm on the kerogen surface, and S_{ma} [m^2/g] is the area of the unfilled macropores.

https://doi.org/10.1021/acs.energyfuels.2c02876
Energy Fuels XXXX, XXX, XXX−XXX

For the sample considered, the lower and upper limits of the mesopore sizes, D_{min} = 6.5 nm and D_{max} = 200 nm, respectively, are determined by the sizes of pores that are filled at the onset of capillary condensation at P/P_0 = 0.6 and at the last measured point on the experimental isotherm at P/P_0 = 0.99. Note that the upper limit of calculated pore size distribution exceeds 50 nm, the conventional maximum diameter of mesopores. The solution of eq 12 is done with the constrain that the total mesopore surface area that includes the areas of filled and unfilled mesopores equal to the total mesopore area of 4.3 m^2/g determined by the comparative plot. The micropore volume is set to zero according to the comparative plot that does not indicate a sizable microporosity in the sample considered. The method of solution of eq 12 is explained in section B of the Supporting Information.

Equation 12 is an ill-posed problem and slight fluctuations in the experimental points can lead to artificial peaks in the pore size distribution. To counter this issue, we interpolate the measured points and fit the experimental isotherm $N_{exp}(P)$ in the range 0.01−0.99 P/P_0 to the Frenkel−Halsey−Hill (FHH) equation $N^{FHH} = N_m (\log(P_0/P))^{-1/s}$ and obtain a nice fit (with N_m = 0.071 mmol/g and s = 2.2). The pore size distribution was calculated based on the FHH function up to P/P_0 = 0.99, which corresponds to a cylindrical pore of size ∼200 nm as predicted by the DBdB approach. Since the minimum size of the mesopores determined from the comparison plot is relatively large (∼6.5 nm), the use of DBdB approach is justifiable for the assessment of the complete range of pores.

The pore size distribution calculated using the DBdB kernel for cylindrical pores are shown in Figure 9c. The sample exhibits a wide pore size distribution with a peak around ∼8 nm. The surface area of unfilled macropores, S_{ma}, is 1.5 m^2/g, and the area of mesopores, S_{me}, is 2.8 m^2/g. This shows that a significant portion of the pore space remains unfilled at the last measured pressure of P/P_0 = 0.99, where the adsorbates in the films covering unfilled pores constitute 12% from the total adsorption. It is worth noting that the sample considered does not possess micropores and small mesopores <6.5 nm. In the case of samples with smaller pores, a hybrid kernel, $K(P/P_0, D)$, should be used composed of QSDFT isotherms in smaller pores (<6 nm) and DBdB isotherms in larger mesopores (<6 nm).

■ CONCLUSIONS

Kerogen fractions of shales possess a hierarchical pore structure with a wide pore size distribution spanning the whole range of micro-, meso-, and macropores. This pore structure heterogeneity is reflected in adsorption isotherms, which in many cases demonstrate a gradual unlimited increase approaching the saturation pressure, as shown by a typical example of N_2 adsorption on the Kimmeridge kerogen sample shown in Figure 9. We suggest a multiscale methodology for constructing realistic molecular models of kerogen micro-porous matrices with embedded mesopores and calculating the adsorption isotherms using a combination of MC simulations, quenched solid density functional theory (QSDFT), and macroscopic Derjaguin−Broekhoff−de Boer (DBdB) theory. The proposed approach allows us to create a kernel of the reference isotherms of adsorption in kerogen micropores, kerogen surface, and mesopores in the range from 2 to 200 nm for calculating the microporosity, surface area, and pore size distribution from experimental adsorption isotherms. As a characteristic example, the kerogen II-A chemical structure is chosen to demonstrate the capabilities of the proposed approach.

Based on Ungerer's model of kerogen II A units,[10] we build the 3D atomistic models of the bulk kerogen matrix and kerogen surface. Using GCMC, we calculate the reference adsorption isotherms of N_2 at 77.4 K in the microporous kerogen matrix and molecularly rough kerogen surface that are further used for pore structure characterization. The effective BET surface calculated from the GCMC isotherm exceeds the geometric projection surface by the factor of 1.5 reflecting the kerogen surface molecular heterogeneity. It is worth noting that the GCMC reference surface isotherm reduced to the BET surface coincides with the standard Harking−Jura (HJ) isotherm in the region 0.05 < P/P_0 < 0.5 but deviates at higher pressures.

The GCMC isotherms generated in the model slit pores between the kerogen surfaces demonstrate the transition from the reversible pore filling in micropores (<2 nm) to pronounced capillary condensation−desorption hysteresis in mesopores as the pore size increases. The adsorption isotherms in mesopores in the region before the capillary condensation coincide with the reference surface isotherm. Further, the GCMC generated adsorption isotherms are used as references for building theoretical models of adsorption on kerogen mesopores.

Based on the kerogen surface density profile, we build a QSDFT model of molecularly rough surface with the roughness parameter δ = 0.7 that is parameterized to reproduce the GCMC reference surface isotherms. A good agreement between QSDFT and GCMC isotherms in slit pores validates the QSDFT parameterization. The QSDFT model allows us to determine the positions of the equilibrium capillary condensation−desorption transition within the hysteresis loops that are unavailable in the GCMC simulations. Furthermore, we parameterize the DBdB model by transforming the reference surface isotherm on the kerogen surface into the effective disjoining pressure isotherm approximated by an exponentially decaying function, $\Pi(t) = Ae^{-t/b}$. Using the DBdB theory, we calculate the positions of equilibrium capillary condensation−desorption transitions and build the adsorption isotherms in mesopores of slit and cylindrical shapes. The DBdB results are found in a close agreement with the QSDFT calculations. It is worth noting that the conventional Kelvin−Cohan equation, which forms the basis of the BJH method, significantly overestimates the pore size dependence of the equilibrium condensation pressures compared with our calculations, which account for the realistic molecular structure of kerogen.

The constructed GCMC, QSDFT, and DBdB isotherms calculated in the wide range of pore sizes represents the kernels of reference isotherms used for calculating pore size distributions from experimental adsorption isotherms. With the example of an experimental isotherm of N_2 on the Kimmeridge kerogen sample, we show the advantages of the proposed approach. We show that the comparison plot based on the reference kerogen surface isotherm allows us to determine the micropore volume, the total surface area of meso- and macropores, and the lower limit of the range of mesopore sizes. The upper limit of pore sizes is determined by the highest experimentally measured pressure. The pore size distribution is calculated using the DBdB kernel of equilibrium isotherms calculated for model cylindrical pores with

https://doi.org/10.1021/acs.energyfuels.2c02876
Energy Fuels XXXX, XXX, XXX−XXX

molecularly rough kerogen walls. Complementing the DBdB kernel with the reference surface isotherm allows us to determine the area of unfilled macropores at the highest experimentally measured pressure.

Further work is needed to develop similar models for other kerogens of different maturity and develop hybrid kernels of reference isotherms. It is desirable to build the QSDFT and DBdB for kerogen of different maturities and chemical composition. The parameters of these models are to be customized for each kerogen to reflect the difference in the sample density and carbon fraction. This will allow for determining from the experimental adsorption isotherm the distribution of different types of kerogen fractions in the sample, as well as the micro-,meso-, and microporosity; meso- and macropore surface area; and pore size distributions. Like the conventional NLDFT and QSDFT methods for carbon, the hybrid kernels for kerogens can be built using model pores of different pore shapes: slit, cylindrical, and spherical. The further advancement of the 3D molecular models will provide a comprehensive characterization of hierarchical porosity in kerogens and shales.

■ ASSOCIATED CONTENT

Supporting Information

The Supporting Information is available free of charge at https://pubs.acs.org/doi/10.1021/acs.energyfuels.2c02876.

Supporting Information with simulation methods, approach to solve adsorption integral equation, comparison of reference surface isotherms, construction of the kerogen matrix structure, and QSDFT and DBdB kernels in cylindrical pores (PDF)

■ AUTHOR INFORMATION

Corresponding Author

Alexander V. Neimark − *Department of Chemical and Biochemical Engineering, Rutgers, The State University of New Jersey, Piscataway, New Jersey 08854, United States;* orcid.org/0000-0002-3443-0389; Email: aneimark@rutgers.edu

Authors

Shivam Parashar − *Department of Chemical and Biochemical Engineering, Rutgers, The State University of New Jersey, Piscataway, New Jersey 08854, United States;* orcid.org/0000-0002-0323-7391

Peter I. Ravikovitch − *ExxonMobil Technology and Engineering Company, Annandale, New Jersey 08801, United States*

Complete contact information is available at: https://pubs.acs.org/10.1021/acs.energyfuels.2c02876

Author Contributions

All authors have given approval to the final version of the manuscript.

Notes

The authors declare no competing financial interest.

■ ACKNOWLEDGMENTS

This work was supported by the National Science Foundation (CBET Grant 18334339) and ExxonMobil Technology and Engineering Company.

■ REFERENCES

(1) Bousige, C.; Ghimbeu, C. M.; Vix-Guterl, C.; Pomerantz, A. E.; Suleimenova, A.; Vaughan, G.; Garbarino, G.; Feygenson, M.; Wildgruber, C.; Ulm, F.-J.; Pellenq, R. J. M.; Coasne, B. Realistic molecular model of kerogen's nanostructure. *Nat. Mater.* **2016**, *15*, 576−582.

(2) King, H. E.; Eberle, A. P. R.; Walters, C. C.; Kliewer, C. E.; Ertas, D.; Huynh, C. Pore Architecture and Connectivity in Gas Shale. *Energy Fuels* **2015**, *29*, 1375−1390.

(3) Wang, R.; Zhang, N.; Liu, X.; Wu, X.; Chen, J.; Ma, L. Characteristics of Pore Volume Distribution and Methane Adsorption on Shales. *Adsorpt. Sci. Technol.* **2015**, *33*, 915−937.

(4) Liang, Z.; Jiang, Z.; Li, Z.; Song, Y.; Gao, F.; Liu, X.; Xiang, S. Nanopores Structure and Multifractal Characterization of Bulk Shale and Isolated Kerogen—An Application in Songliao Basin, China. *Energy Fuels* **2021**, *35*, 5818−5842.

(5) Suleimenova, A.; Bake, K. D.; Ozkan, A.; Valenza, J. J.; Kleinberg, R. L.; Burnham, A. K.; Ferralis, N.; Pomerantz, A. E. Acid demineralization with critical point drying: A method for kerogen isolation that preserves microstructure. *Fuel* **2014**, *135*, 492−497.

(6) Valenza, J. J.; Drenzek, N.; Marques, F.; Pagels, M.; Mastalerz, M. Geochemical controls on shale microstructure. *Geology* **2013**, *41*, 611−614.

(7) Kuila, U.; Prasad, M. Specific surface area and pore-size distribution in clays and shales. *Geophys. Prospect.* **2013**, *61*, 341−362.

(8) Xiong, J.; Liu, X.; Liang, L.; Zeng, Q. Methane Adsorption on Carbon Models of the Organic Matter of Organic-Rich Shales. *Energy Fuels* **2017**, *31*, 1489−1501.

(9) Eberle, A. P. R.; King, H. E.; Ravikovitch, P. I.; Walters, C. C.; Rother, G.; Wesolowski, D. J. Direct Measure of the Dense Methane Phase in Gas Shale Organic Porosity by Neutron Scattering. *Energy & Fuels* **2016**, *30*, 9022−9027.

(10) Ungerer, P.; Collell, J.; Yiannourakou, M. Molecular Modeling of the Volumetric and Thermodynamic Properties of Kerogen: Influence of Organic Type and Maturity. *Energy Fuels* **2015**, *29*, 91−105.

(11) Kelemen, S. R.; Afeworki, M.; Gorbaty, M. L.; Sansone, M.; Kwiatek, P. J.; Walters, C. C.; Freund, H.; Siskin, M.; Bence, A. E.; Curry, D. J.; Solum, M.; Pugmire, R. J.; Vandenbroucke, M.; Leblond, M.; Behar, F. Direct Characterization of Kerogen by X-ray and Solid-State 13C Nuclear Magnetic Resonance Methods. *Energy Fuels* **2007**, *21*, 1548−1561.

(12) Wang, T.-Y.; Tian, S.-C.; Liu, Q.-L.; Li, G.-S.; Sheng, M.; Ren, W.-X.; Zhang, P.-P. Pore structure characterization and its effect on methane adsorption in shale kerogen. *Pet. Sci.* **2021**, *18*, 565−578.

(13) Obliger, A.; Ulm, F.-J.; Pellenq, R. Impact of Nanoporosity on Hydrocarbon Transport in Shales' Organic Matter. *Nano Lett.* **2018**, *18*, 832−837.

(14) Phan, A.; Striolo, A. Evidence of Facilitated Transport in Crowded Nanopores. *J. Phys. Chem. Lett.* **2020**, *11*, 1814−1821.

(15) Liu, J.; Chapman, W. G. Thermodynamic Modeling of the Equilibrium Partitioning of Hydrocarbons in Nanoporous Kerogen Particles. *Energy Fuels* **2019**, *33*, 891−904.

(16) Broekhoff, J. C. P.; de Boer, J. H. Studies on pore systems in catalysts: XIV. Calculation of the cumulative distribution functions for slit-shaped pores from the desorption branch of a nitrogen sorption isotherm. *J. Catal.* **1968**, *10*, 391−400.

(17) Broekhoff, J. C. P.; de Boer, J. H. Studies on pore systems in catalysts: XII. Pore distributions from the desorption branch of a nitrogen sorption isotherm in the case of cylindrical pores A. An analysis of the capillary evaporation process. *Journal of Catalysis* **1968**, *10* (4), 368−376.

(18) Neimark, A. V.; Lin, Y.; Ravikovitch, P. I.; Thommes, M. Quenched solid density functional theory and pore size analysis of micro-mesoporous carbons. *Carbon* **2009**, *47*, 1617−1628.

(19) Gor, G. Y.; Thommes, M.; Cychosz, K. A.; Neimark, A. V. Quenched solid density functional theory method for characterization of mesoporous carbons by nitrogen adsorption. *Carbon* **2012**, *50*, 1583−1590.

(20) Zhao, H.; Lai, Z.; Firoozabadi, A. Sorption Hysteresis of Light Hydrocarbons and Carbon Dioxide in Shale and Kerogen. *Sci. Rep.* **2017**, *7*, No. 16209.

(21) Collell, J.; Ungerer, P.; Galliero, G.; Yiannourakou, M.; Montel, F.; Pujol, M. Molecular Simulation of Bulk Organic Matter in Type II Shales in the Middle of the Oil Formation Window. *Energy Fuels* **2014**, *28*, 7457−7466.

(22) Okiongbo, K. S.; Aplin, A. C.; Larter, S. R. Changes in Type II Kerogen Density as a Function of Maturity: Evidence from the Kimmeridge Clay Formation. *Energy Fuels* **2005**, *19*, 2495−2499.

(23) Wang, J.; Wolf, R. M.; Caldwell, J. W.; Kollman, P. A.; Case, D. A. Development and testing of a general amber force field. *J. Comput. Chem.* **2004**, *25*, 1157−1174.

(24) Plimpton, S. Fast Parallel Algorithms for Short-Range Molecular Dynamics. *J. Comput. Phys.* **1995**, *117*, 1−19.

(25) Rappe, A. K.; Goddard, W. A. Charge equilibration for molecular dynamics simulations. *J. Phys. Chem. A* **1991**, *95*, 3358−3363.

(26) Dubbeldam, D.; Calero, S.; Ellis, D. E.; Snurr, R. Q. RASPA: Molecular simulation software for adsorption and diffusion in flexible nanoporous materials. *Mol. Simul.* **2016**, *42*, 81−101.

(27) Okiongbo, K. S.; Aplin, A. C.; Larter, S. R. Changes in type II kerogen density as a function of maturity: Evidence from the Kimmeridge Clay Formation. *Energy Fuels* **2005**, *19*, 2495−2499.

(28) Sarkisov, L.; Harrison, A. Computational structure characterisation tools in application to ordered and disordered porous materials. *Mol. Simul.* **2011**, *37*, 1248−1257.

(29) Potoff, J. J.; Siepmann, J. I. Vapor−liquid equilibria of mixtures containing alkanes, carbon dioxide, and nitrogen. *AIChE J.* **2001**, *47*, 1676−1682.

(30) Mayo, S. L.; Olafson, B. D.; Goddard, W. A. Dreiding - a Generic Force-Field for Molecular Simulations. *J. Phys. Chem. C* **1990**, *94*, 8897−8909.

(31) Ungerer, P.; Tavitian, B.; Boutin, A. *Application of Molecular Simulation in the Oil and Gas Industry. Monte Carlo Methods*; Editions TECHNIP, 2005.

(32) Psarras, P.; Holmes, R.; Vishal, V.; Wilcox, J. Methane and CO2 Adsorption Capacities of Kerogen in the Eagle Ford Shale from Molecular Simulation. *Acc. Chem. Res.* **2017**, *50*, 1818−1828.

(33) Neimark, A. V.; Vishnyakov, A. Gauge cell method for simulation studies of phase transitions in confined systems. *Physical Review E* **2000**, *62*, 4611−4622.

(34) Vishnyakov, A.; Neimark, A. V. Studies of Liquid−Vapor Equilibria, Criticality, and Spinodal Transitions in Nanopores by the Gauge Cell Monte Carlo Simulation Method. *J. Phys. Chem. B* **2001**, *105*, 7009−7020.

(35) Neimark, A. V.; Vishnyakov, A. A simulation method for the calculation of chemical potentials in small, inhomogeneous, and dense systems. *J. Chem. Phys.* **2005**, *122*, No. 234108.

(36) Widom, B. Some Topics in the Theory of Fluids. *J. Chem. Phys.* **1963**, *39*, 2808−2812.

(37) Ravikovitch, P. I.; Neimark, A. V. Density Functional Theory Model of Adsorption on Amorphous and Microporous Silica Materials. *Langmuir* **2006**, *22*, 11171−11179.

(38) Ravikovitch, P. I.; Neimark, A. V. Density Functional Theory of Adsorption in Spherical Cavities and Pore Size Characterization of Templated Nanoporous Silicas with Cubic and Three-Dimensional Hexagonal Structures. *Langmuir* **2002**, *18*, 1550−1560.

(39) Harkins, W. D.; Jura, G. An adsorption method for the determination of the area of a solid without the assumption of a molecular area, and the area occupied by nitrogen molecules on the surfaces of solids. *The Journal of Chemical Physics* **1943**, *11*, 431.

(40) Weeks, J. D.; Chandler, D.; Andersen, H. C. Role of Repulsive Forces in Determining the Equilibrium Structure of Simple Liquids. *J. Chem. Phys.* **1971**, *54*, 5237−5247.

(41) Schlangen, L. J. M.; Koopal, L. K.; Stuart, M. A. C.; Lyklema, J.; Robin, M.; Toulhoat, H. Thin Hydrocarbon and Water Films on Bare and Methylated Silica: Vapor Adsorption, Wettability, Adhesion, and Surface Forces. *Langmuir* **1995**, *11*, 1701−1710.

(42) Ravikovitch, P. I.; Vishnyakov, A.; Neimark, A. V.; Ribeiro Carrott, M. M. L.; Russo, P. A.; Carrott, P. J. Characterization of Micro-Mesoporous Materials from Nitrogen and Toluene Adsorption: Experiment and Modeling. *Langmuir* **2006**, *22*, 513−516.

(43) Gor, G. Y.; Paris, O.; Prass, J.; Russo, P. A.; Ribeiro Carrott, M. M. L.; Neimark, A. V. Adsorption of n-Pentane on Mesoporous Silica and Adsorbent Deformation. *Langmuir* **2013**, *29*, 8601−8608.

(44) Barrett, E. P.; Joyner, L. G.; Halenda, P. P. The Determination of Pore Volume and Area Distributions in Porous Substances. I. Computations from Nitrogen Isotherms. *J. Am. Chem. Soc.* **1951**, *73*, 373−380.

(45) Harkins, W. D.; Jura, G. Surfaces of Solids. XII. An Absolute Method for the Determination of the Area of a Finely Divided Crystalline Solid. *J. Am. Chem. Soc.* **1944**, *66*, 1362−1366.

https://doi.org/10.1021/acs.energyfuels.2c02876
Energy Fuels XXXX, XXX, XXX−XXX